Dynamic Characterization of Crystalline Supramolecular Rotors Assembled through Halogen Bonding

Luca Catalano,[1,2] Salvador Pérez-Estrada,[2] Giancarlo Terraneo,[1]* Tullio Pilati,[1] Giuseppe Resnati,[1] Pierangelo Metrangolo, [1,3]* and Miguel A. Garcia-Garibay[2]*

[1] Laboratory of Nanostructured Fluorinated Materials (NFMLab), Department of Chemistry, Materials, and Chemical Engineering "Giulio Natta", Politecnico di Milano, via L. Mancinelli 7, 20131 Milano, Italy;

[2] Department of Chemistry and Biochemistry, University of California, Los Angeles, California 90095-1569, USA;

[3] VTT-Technical Research Centre of Finland, PO Box 1000, Espoo FI-02044, Finland.

Amphidynamic crystals are materials specifically designed to possess rapidly moving components (rotators) in the solid state.[1] It is expected that these materials may provide a suitable platform for the development of future functional materials and artificial molecular machines.[1,2] Typically, molecular design in this field has taken inspiration from structures akin to those of macroscopic compasses and gyroscopes to explore and control rotation in the solid state.[3] Rotation in solids has been studied in molecular crystals,[3] inclusion compounds,[4] metal organic frameworks (MOFs),[5] porous molecularly ordered (PMO) silicates,[6] and amorphous solids.[7]

Here we take advantage of the principles of crystal engineering[8] to assemble stators and rotators into cocrystals, which results in the high-yield synthesis of active supramolecular rotor arrays. Advantages of this strategy originate from the intrinsic flexibility and its modular design, thanks to the wide variety of supramolecular synthons[8] available in the crystal engineering toolbox. Furthermore, the dynamic performance of the supramolecular rotor may be tuned by controlling the noncovalent interactions involving stators and rotators in the crystal structures.

Among the wide variety of noncovalent interactions available, such as metal coordination, Coulombic interactions, hydrogen bonding (HB), and π-π stacking, halogen bonding has only been used once for the design of amphidynamic crystals.[9,10] In particular, it was demonstrated recently that bis(1,4-iodoethynyl) bicyclo[2.2.2]octane (**BIBCO**) showed ultrafast rotation when self-assembled in crystalline halogen-bonded networks through iodine-acetylene interactions at the two ends of each rotator.[11] Under the hypothesis that the halogen bond, thanks to its strength, directionality, selectivity, and tunability, may provide an extra value in the design of cocrystals showing dynamic components, we studied molecular motions of a series of halogen-bonded cocrystals involving 1,4-diazabicylo[2.2.2]-octane (**DABCO**)[12], a well-known *C*3-symmetric and cylindrically-shaped rotator that packs in a manner that does not generate high rotational barriers.[11,13]

The commercially available fluorosubstituted iodobenzenes (F_nPheI) **1a-e** were chosen as powerful halogen bond (XB) donors that can play the role of stators when assembled with the **DABCO** rotator *via* F_nPheI···NR_3 interactions (Figure 1). We anticipated that compounds **1a-e** would simultaneously offer a suitable static platform, a noncovalent axle, the XB, and a frame of reference for the rotation of **DABCO**.

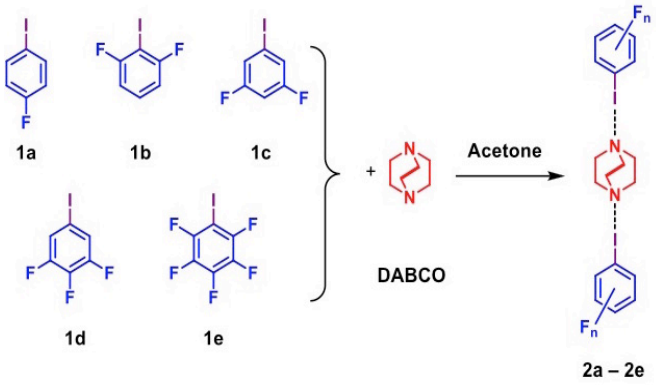

Figure 1. The self-assembly of the fluorosubstituted iodobenzenes (F_nPheI) **1a-e** and **DABCO** resulted in crystalline halogen-bonded molecular rotors **2a-e**.

Self-assembly experiments were carried out by mixing in acetone solutions two equivalents of **1a-1e** per equivalent of **DABCO**, taking into account the mono- and bidentate nature of **1a-1e** and **DABCO**, respectively, as far as the XB-donor/acceptor sites are concerned. Upon slow solvent evaporation, crystalline solids were obtained in all cases with melting points different from the starting compounds and ranging from 311 K to 378 K (Table 1). Peak integration of the ^{1}H NMR spectra confirmed that all of the complexes but **2c**, showed the expected 2:1 ratios of the

starting compounds. The complex **2c**, instead, showed a 1:1 ratio between **1c** and **DABCO**.

Table 1. Melting points, space groups, and Arrhenius parameters for rotational dynamics from the Kubo-Tomita fit of the T_1 data for **DABCO** and the related halogen-bonded cocrystals (**2a-e**).

Compound/cocrystal (m.p. / K)	Space group (Z)[a]	E_a (kcal/mol)	τ_0^{-1} (s^{-1})	C (s^{-2})
DABCO (429)	$P6_3/m$[b] (2)	8.2[c]	$1.3x10^{14}$ [c]	n.a.
2a (318-321)	C2/c (4)	4.8	$9.9x10^{12}$	$5.2x10^{8}$
2b (334-336)	$P2_1/n$ (4)	2.7	$2.0x10^{12}$	$7.4x10^{8}$
2c (344-345)	$P2_1/c$ (4)	2.4	$1.1x10^{12}$	$6.5x10^{8}$
2d (311-314)	$P2_1/c$ (2)	2.8	$2.3x10^{12}$	$5.0x10^{8}$
2e (377-378)	$P2_1/c$ (2)	3.6	$2.3x10^{12}$	$7.5x10^{8}$

[a] Data obtained at 297 K, Z is the number of molecules per asymmetric unit; [b] Reference 14a; [c] Reference 14b.

Good-quality single crystals of the obtained cocrystals **2a-e** were submitted to X-ray diffraction (XRD) analysis, which was in all cases carried out at 103 K. Structural analysis confirmed the starting design of the desired halogen-bonded motif with both the N atoms of **DABCO** working as XB-acceptors towards the I atoms of two different F_nPheI modules, resulting in trimeric complexes. Differently, the structure of the complex **2c** consisted of 1D infinite chains where **1c** and **DABCO** alternated as a consequence of the bidentate nature of **1c**, which also behaved as HB-donor through the H atom in the *p* position to the I atom in the benzene ring (Figure 2b). This explains the 1:1 ratio observed for this complex through ^{1}H NMR analysis, which was obtained from both starting from either 1:1 or 2:1 mixing ratios.

Table 2. XB Geometrical features in **2a-e** at 103 K.

Complex	N···I (Å)	N···I-C angle (°)
2a	2.971 (4), 2.955 (4)[a]	176.32 (2), 175.51 (2)[a]
2b	2.857 (2), 2.732 (2) [a]	173.86 (8), 179.12 (8) [a]
2c	2.832 (1)	175.19 (4)
2d	2.815 (6)	175.8 (2)
2e	2.713 (1), 2.682 (1), 2.681 (1), 2.701 (1)[a]	177.04 (5), 178.64 (5), 177.96 (5), 177.19 (5)[a]

[a] Independent halogen bonds;

The XBs observed in the complexes **2a-e** are characterized by short I···N distances (2.79 Å on average) and almost linear C-I···N angles (176.7 ° on average), as shown in Table 2. The XB becomes shorter, namely stronger, with the increase of the fluorination degree of the stator, and hence the magnitude of the iodine σ -hole.[16] Similarly, *m*-fluorination may explain why **1c** behaves as HB-donor, while **1b** doesn't. No other driving noncovalent interactions characterize the crystal packing of these complexes.[15] Importantly, NMR, IR, thermal, and Powder XRD analyses confirmed the quantitative bulk obtainment of the above-described cocrystals.

In order to explore structural changes and the dynamics of **DABCO** in the complexes **2a-e** when varying the temperature, we performed variable-temperature (VT) single-crystal XRD, VT ^{1}H T_1 NMR, and VT wide-line quadrupolar echo ^{2}H NMR analyses. It is known that changes in the size and orientation of the anisotropic thermal parameters, may be related to the potential energy that determines dynamic processes in crystals.[16] On heating up single crystals of the complexes **2a** and **2e** from *ca.* 100 K

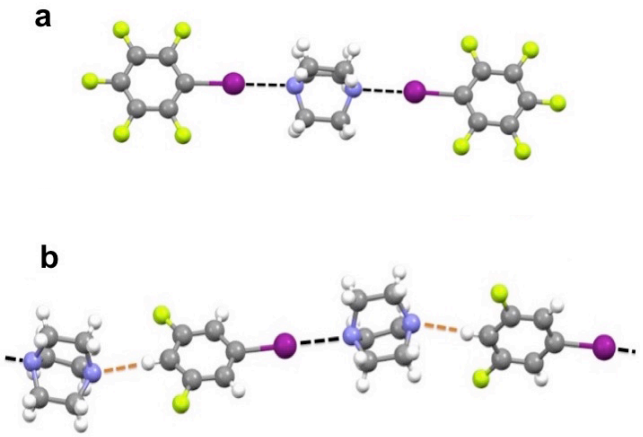

Figure 2. (a) Halogen-bonded trimer in the crystal structure of **2e** and (b) 1D infinite chain in **2c** due to the simultaneous XB and HB donor behaviour of **1c** when mixed with **DABCO**. HB geometrical parameters are as follows: C···N distance 3.348(3) Å and C-H···N angle 174.0(1)°. Color code: C, gray; H, white; N, sky blue; F, light green; I, magenta. XB and HB are represented as black and orange dashed lines, respectively.

to room temperature, reversible phase transitions without substantial modifications of the crystal packing were recorded. These occurred at *ca.* 280 K and 230 K, respectively, as shown in detail in the Supporting Information (SI) section. For **2e**, XRD data were collected in the range 103-298 K, following five intermediate steps (140, 180, 200, 220, and 250 K). On increasing the temperature of the XRD acquisition experiment, increasing rotational disordered of the **DABCO** -CH_2CH_2- alkyl bridges was observed, which has to be expected from a thermally activated rotational process (Figure 3). Conversely, the pentafluoroiodobenzene module only showed disorder in the plane of the aromatic ring (see SI). Similar motion and disorder were also observed for the cocrystals **2a-d**.

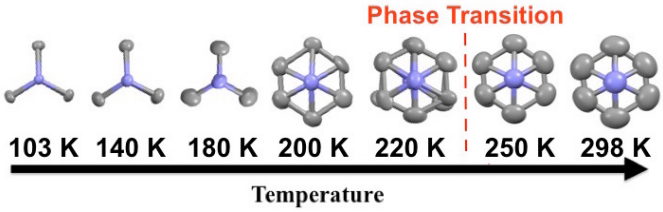

Figure 3. Views along the N-N axis of the **DABCO** component in cocrystal **2e**, which show increasing disorder of the alkyl bridges, in terms of larger thermal ellipsoids and splitting over two positions as a function of temperature from 103 K to 298 K.

Spin lattice relaxation measurements have been used to document dynamic processes in the vicinity of the Larmor frequency[18] (300 MHz for ^{1}H T_1 measurements in this case). This method is well suited for crystalline solids where the main mechanism of relaxation is due to the motion-mediated fluctuation of magnetic fields arising from dipolar coupling among hydrogen atoms. In the case of the cocrystals **2a-e**, the rotation of **DABCO** is the predominant thermally-activated process with dynamics characterized by a correlation time (τ_c), which follows an Arrhenius-type behavior (Eq. 1). Under these conditions, it is possible to obtain its activation energy (E_a) and pre-exponential factor (τ_0^{-1}) by fitting the measured T_1 data as a function of temperature to the Ku-

bo-Tomita (K-T) relaxation expression (Eq. 2), by substituting the τ_c term with Eq. 1.

$$\tau_c^{-1} = \tau_0^{-1} \exp(-E_a/RT) \quad \text{(Eq. 1)}$$

$$T_1^{-1} = C\,[\tau_c(1+\omega_0^2\,\tau_c^2)^{-1} + 4\tau_c(1+4\,\omega_0^2\,\tau_c^2)^{-1}] \quad \text{(Eq. 2)}$$

The parameter C in Eq. 2 is a constant related to the strength of the homonuclear dipolar interactions, which, as expected, is similar for all of the studied cocrystals (see Table 1), and ω_0 is the Larmor frequency (for further details, please, refer to the SI). Good K-T fitting of the experimental data were obtained, allowing the determination of the Arrhenius parameters reported in Table 1.

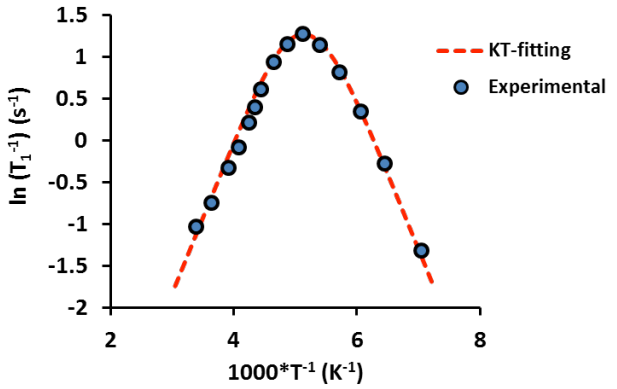

Figure 4. ^{1}H spin-lattice relaxation times (^{1}H T_1) measured for **2e** on cooling from 295 K to 141 K at 300 MHz (solid blue circles). The plot $\ln(T_1^{-1})$ *vs.* $1000T^{-1}$ shows a maximum at approximately 195 K. The red dotted line corresponds to the Kubo-Tomita fit of the experimental data.

As illustrated in the Figure 4 with a $\ln(T_1^{-1})$ *vs.* 1000/T(K) plot of the experimental data obtained on cocrystal **2e**, there is a single maximum at *ca.* 195 K with an excellent K-T fit for a single dynamic process with an exceptionally low energy of activation of around 3.6 kcal/mol and a pre-exponential factor $\tau_o = 2.3\text{x}10^{12}$ s^{-1}. Similar behaviors were obtained also for **2a-d** with activation energies ranging from 2.4 to 4.9 kcal/mol (Table 1). Notably, data obtained from cocrystal **2a** showed a discontinuity that correlates with a phase transition that occurs in the range 285-310 K (Figure S17). While it was not possible to fit the experimental data in the high temperature phase due to the small number of experimental points in the proximity of the crystal melting, the dynamics of the low temperature phase was fully characterized with an E_a = 4.9 kcal/mol and $\tau_o = 9.9\text{x}10^{12}$ s^{-1}.

The activation energies measured for cocrystals **2a-e** are considerably lower than the activation energy for rotation reported in the case of pure crystalline **DABCO**, which has an E_a =8.2 kcal/mol and $\tau_o = 1.3\text{x}10^{14}$ s^{-1} (Table 1). This may probably be due to the fact that rotator molecules in the reported halogen-bonded cocrystals are partially isolated from neighboring rotators by the XB-donors **1a-e**, which thus function as bearings and stators (Figure 5).

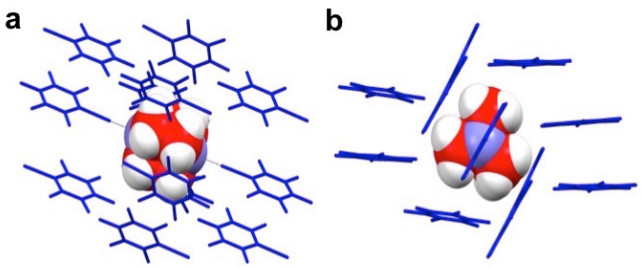

Figure 5. Views along the *b* crystallographic axis (a) and along the N-N molecular axis (b) of the crystal structure of **2e**, showing the isolation of a **DABCO** rotator (red) by neighboring pentafluoroiodobenzene modules in blue.

The higher activation energy for rotation of pure **DABCO** may be associated with the closer rotator-rotator distances and steric interactions in the crystal. The pre-exponential factor τ_0^{-1} is related to the frequency of oscillations within the local energy well, and can be associated with an attempt frequency for rotational jumps that is determined both by thermal energy and the size of the activation barrier ($-E_a$/RT). The attempt frequency corresponds to the rotational exchange frequency that would occur in the absence of a barrier, *i.e.*, when E_a =0. Notably, the τ_0^{-1} values obtained for the halogen-bonded cocrystals **2a-e** are comparable to those determined for other amphidynamic crystals with analogous **DABCO**-based molecular rotators linked to the stators by covalent bonds.[11,13] This suggests that the halogen-bonded molecular rotors reported in this paper may be as efficient as similar rotors based fully on covalent bonds. However, in cocrystal **2c**, it was not possible to discern the different contributions of XB and HB to the rotational dynamics of the supramolecular rotor.

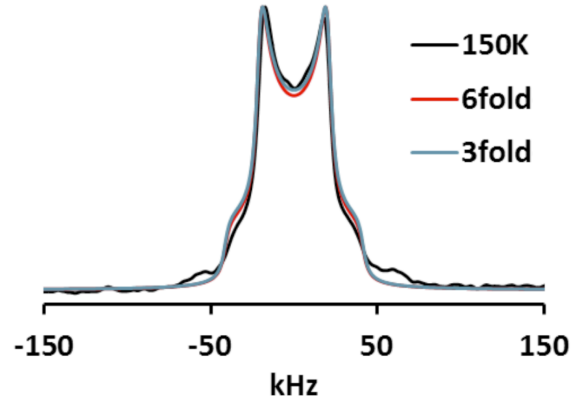

Figure 6. Deuterium wide line spectrum of **2a** collected at 150 K (black line) compared with 3-fold and 6-fold potential simulated spectra (blue and red lines).

To elucidate the trajectories of motion, three supramolecular rotors (**2a**, **2b**,and **2e**) were taken as models and their dynamics studied by wide-line quadrupolar echo ^{2}H NMR.[18] The sample cocrystals were prepared by using perdeuterated **DABCO** obtained by H/D exchange reaction using Raney Nickel and D_2O.[19] For the three studied systems the wide line spectra collected between 140 K and 295 K did not show any appreciable changes, in good agreement with the high rotational frequencies expected from the low E_a and high τ_o values. The simulated spectra[20] suggested a dynamical process where **DABCO** rotates around its N-N axis in the fast-exchange regime. The experimental data coupled with the simulations are consistent with both a 3-site or 6-site potential of the rotator, see example in Figure 6.

In conclusion, a series of two-component amphidynamic cocrystals with very efficient rotational dynamics were readily prepared from simple and commercially available building blocks by taking advantage of a crystal engineering strategy based on the use of halogen bonding. The reported systems are the first examples of this new class of materials. Rotational dynamics based on VT ^{1}H T_1 NMR spin-lattice relaxation revealed pre-exponential factors comparable to those found in rotors with covalent rotational axles, suggesting that the XB, and the HB in the specific case of **2c**, constitute new robust axles for molecular rotation and a new design principle in the field of molecular rotors. The discovery of these new crystalline multicomponent systems opens,

TOC

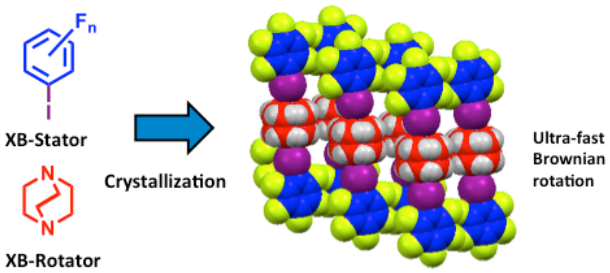

thus, up new avenues in the development of new smart materials and molecular machines.

ASSOCIATED CONTENT

Supporting Information

Experimental procedures, further characterization, and images of spectra. This material is available free of charge via the Internet at http://pubs.acs.org.

AUTHOR INFORMATION

Corresponding Authors
giancarlo.terraneo@polimi.it;
pierangelo.metrangolo@polimi.it; mgg@chem.ucla.edu

Notes

The authors declare no competing financial interest.

ACKNOWLEDGMENTS

MGG acknowledges support from the National Science Founda-tion (grant DMR1402682). PM and GT acknowledge support from the MIUR, PRIN 2010-2011 (grant 2010CX2TLM "In-foChem").

REFERENCES

(1) Vogelsberg, C. S.; Garcia-Garibay, M. *Chem. Soc. Rev.* **2012**, *41*, 1892-1910.
(2) (a) Akutagawa, T.; Shitagami, K.; Nishihara, S.; Takeda, S.; Hasegawa, T.; Nakamura, T.; Hosokoshi, Y.; Inoue, K.; Ikeuchi, S.;Miyazaki, Y; Saito, K. *J. Am. Chem. Soc.* **2005**, *127*, 4397-4402; (b) Kottas, G. S.; Clarke, L. I.; Horinek, D.; Michl, J. *Chem. Rev.* **2005**, *105*, 1281-1376; (c) Akutagawa, T.; Koshinaka, H.; Sato, D.; Takeda, S.; Noro, S.-I.; Takahashi, H.; Kumai, R.; Tokura, Y.; Nakamura, T. *Nat. Mat.* **2009**, *8*, 342-347; (d) Hou, X.; Ke, C.; Bruns, C. J.; Mc Gonigal, P. R.; Pettman, R. B.; Stoddart, J. F. *Nat. Commun*. **2015**, *6*, 6884. (e) Zhu, K.; O'Keefe, C. A.; Vukotic, V. N.; Shurko, R. W., Loeb, S. J. *Nat. Chem.* **2015**, *7*, 514-519.
(3) (a) Dominguez, Z.; Dang, H.; Strouse, M.J.; Garcia-Garibay, M.A *J. Am. Chem. Soc*. **2002**, 124, 2398-2399; (b) Comotti, A.; Bracco, S.; Yamamoto, A.; Beretta, M.; Hirukawa, T.; Tohnai, M.; Miyata, M.; Sozzani, P. *J. Am. Chem. Soc.* **2014**, *136*, 618-621.
(4) Kobr, L.; Zhao, K.; Shen, Y.; Comotti, A.; Bracco, S.; Shoemaker, R.K.; Sozzani, P.; Clark, N.A.; Price, J.C.; Rogers, C.T.; Michl J. *J. Am. Chem. Soc*. **2012**, *134*, 10122–10131.
(5) (a) Gould, S.L.; Tranchemontagne, D.; Yaghi, O.M.; Garcia-Garibay, M.A. *J. Am. Chem. Soc.* **2008**, *130*, 3246-3247; (b) Winston, E.B.; Lowell, P.J.; Vacek, J.; Chocholoušová, J.; Michl, J.; Price, J.C. *Physical Chemistry Chemical Physics,* **2008**, *10*, 5188. (c) Kolokolov, D.I., Stepanov, A.G.; Jobic, H. *J. Phys. Chem. C,* **2014**, *118*, 15978-15984; Shustova, N.B.; McCarthy, B.D.; Dincă, M. *J. Am. Chem. Soc.* **2011**, *133*, 20126-20129.
(6) (a) Bracco, S.; Comotti, A.; Valsesia, P.; Chmelka, B.F.; Sozzani, P. *Chem. Commun.* **2008**, 4798-4800; (b) Bracco, S.; Beretta, M.; Cattaneo, A.; Comotti, A.; Falqui, A.; Zhao, K.; Rogers, C.; Sozzani, P. *Angew. Chem. Int. Ed.* **2015**, *54*, 4773-4777; (c) Vogelsberg, C.S.; Bracco, S.; Beretta, M.; Comotti, A.; Sozzani, P.; Garcia-Garibay, M.A. *J. Phys. Chem. B*. **2012**, *116*, 1623–1632; (d) Comotti, A.; Bracco, S.; Valsesia, P.; Beretta, M.; Sozzani, P. *Angew. Chem., Int. Ed.* **2010**, 49, 1760– 1764.
(7) (a) O'Brien, Z.J.; Karlen, S.D.; Khan, S.; Garcia-Garibay, M.A. *J. Org. Chem.*, 2010, *75*, 2482-2491; (b) Comotti, A.; Bracco, S.; Ben, T.; Qiu, S.; Sozzani, P. *Angew. Chem. Int. Ed.* **2014**, *53*, 1043-1047.
(8) Desiraju, G. R. *Angew. Chem. Int. Ed.* **1995**, *34*, 2311-2327.
(9) Torres-Huerta, A.; Rodríguez-Molina, B.; Höpfl, H.; Garcia-Garibay, M.A. *Organometallics*, **2014**, *33*, 354–362.
(10) (a) Corradi, E.; Meille, S. V.; Messina, M. T.; Metrangolo, P.; Resnati G. *Angew. Chem. Int. Ed.* **2000**, *39*, 1782-1786. (b) Metrangolo, P.; Resnati, G. *Chem. Eur. J.* **2001**, *7*, 2511-2519. (c) Metrangolo, P.; Meyer, F.; Pilati, T.; Resnati, G.; Terraneo, G. *Angew. Chem. Int. Ed.* **2008**, *47*, 6114-6127. (d) Priimagi, A.; Cavallo, G.; Metrangolo, P.; Resnati, G. *Acc. Chem. Res.* **2013**, *46*, 26862695.
(11) Lemouchi, C.; Vogelsberg, C. S.; Zorina, L.; Simonov, S.; Batail, P.; Brown, S.; Garcia-Garibay, M. *J. Am. Chem. Soc.* **2011**, *133*, 6371-6379.
(12) Le Questel, J.-Y.; Laurence, C.; Graton, J. *CrystEngComm* **2013**, *15*, 3212-3221.
(13) (a) Karlen, S. D.; Reyes, H.; Taylor, R. E.; Khan, S. I; Hawthorne, M. F; Garcia-Garibay, M. *Proc. Nat. Ac. Sc.* **2010**, *107*, 14973-14977. (b) Rodriguez-Molina, B.; Perez-Estrada, S.; Garcia-Garibay, M.A. *J. Am. Chem. Soc*., **2013**, *135*, 10388–10395.
(14) (a) Sauvajol, J. L. *J. Phys. C: Solid St. Phys.* **1980**, *13*, 927-934. (b) Zussman, A; Alexander, S. *J. Chem. Phys.* **1967**, *48*, 3534-3539.
(15) (a) Cho, D. M.; Parkin, S. R.; Watson, M. D. *Org. Lett* **2005**, *7*, 1067-1068. (b) Shishkin, O. V.; Shishkina, S. V.; Maleev, A. V.; Zubatyuk, R. I.; Vasylyeva, V.; Merz, K. *ChemPhysChem* **2013**, *14*, 847-856.
(16) Politzer, P.; Murray, J. S.; Clark, T. *Phys.Chem.Chem.Phys.*, **2013**, *15*, 11178-11189.
(17) (a) Dunitz, J. D.; Schomaker, V.; Trueblood, K. N. *J. Phys. Chem.* **1988**, 92, 856. (b) Dunitz, J.; Maverick, E. F.; Trueblood, K. N. *Angew. Chem., Int. Ed. Engl.* **1988**, *27*, 880-895.
(18) Fyfe, C. A. *Solid State NMR for Chemists*; C.F.C Press: Guelph, Ontario, 1983.
(19) Dinnocenzo, J. P.; Banach, T. E. *J. Am. Chem. Soc.* **1988**, *110*, 971-973.
(20) Nishikiori, S. I.; Soma, T.; Iwamoto, T. *J. Inclusion Phenom. Mol. Recognit. Chem.* **1997**, *27*, 233.